MALAYSIAN JOURNAL OF SCIENCE
MJS
ISSN 1394-3065

Regular Issue

Malaysian Journal of Science 43 (1): 11-21 (Mar 2024) https://mjs.um.edu.my

ASSESSING LOCAL PORE WATER VELOCITY ALONG PREFERENTIAL FLOW IN EARTHEN DAM USING SALT TRACER

Huong Thi Thu Huynh[1a]*, Son Le Van[2a], Hieu Tran Trong[3a], Luan Phan Thi[4a], Phung Vuong Duc[5a] and Hai Lai Viet[6a]

Abstract: The local pore water velocity along the preferential flow path signifies the hydraulic parameter responsible for erosion within an earthen dam. This study introduces an empirical approach to ascertain the local pore water velocity within the earth dam's leakage zones by monitoring the travel time of the salt tracer through the corresponding electric potential anomalies in the ground. The alignment of electric potential anomalies with the movement of the salt tracer plume over time was confirmed through experiments on a physical model coupled with numerical simulations. The pore water velocity, calculated based on the location of the maximum electric potential anomaly, demonstrated excellent agreement with the experimental value, with an error of under 6%. For illustrative purposes, a field-scale salt tracer test was conducted at a leaking earthen dam in Vietnam. The tracer breakthrough curve originating from the leakage point revealed that the seepage water's travel time is approximately 40 days. The results of electric potential anomalies over time indicate that the pathway of seepage flow from upstream to the leakage point forms a horizontal V-shape, with the local pore water velocity ranging from 1.7 to 9.9x10^{-5} m/s. These local pore water velocities are subsequently compared with the critical seepage velocity to assess in-situ information regarding the internal erosion status of the target dam.

Keywords: *Leakage, internal erosion, salt tracer, electric potential*

1. Introduction

Concentrated seepage resulting from local permeability anomalies in the body and foundation of an earthen dam is one of the primary mechanisms responsible for internal erosion (Foster et al., 2000; Zhang et al., 2016). Statistics based on the International Commission on Large Dams (ICOLD) database, comprising more than 10,000 dams, reveal that seepage erosion accounts for approximately 50% of dam failures (Foster et al., 1998). Detecting abnormal downstream leaks necessitates serious consideration of erosion potential to prevent or mitigate the damage caused by dam failures. Erosion occurs when the seepage water velocity is sufficiently high to transport discrete fine soil particles through the pores. Hence, the local pore water velocity along the preferential flow path serves as a hydraulic parameter for assessing the erosion process within the earthen dam (Goltz et al., 2009).

While geophysical methods for dam investigation, such as radar (Hui & Haitao, 2011; Bigman & Day, 2022), micro-seismic (Hickey et al., 2010), and resistivity (Kukemilks & Wagner, 2021; Zumr et al., 2020), focus on providing a visual representation of the seepage zone, the tracer method is considered an empirical technique that enables the determination of flow path direction and water velocity in the dam body and foundation (Bedmar & Araguas, 2002; Qiu et al., 2022). A tracer test is conducted by introducing artificial tracers like saline, ethanol, or fluorescent substances at a known upstream location and monitoring their concentration over time at target sites such as piezometers and downstream leakage points. The water velocity in the preferential flow can be determined using the tracer concentration curves at the monitoring locations. For instance, Battaglia et al. (2016) located the leakage zone at the Bumbuna dam by analyzing arrival times and tracer recovery in a series of experiments employing fluorescent dyes. Noraee Nejad et al. (2021) utilized a tracer experiment with $NaNO_3$ salt to investigate seepage at Shahghasem dam, determining the primary flow direction of the preferential flow path based on flow velocity calculations from experimental tracer curves. Sampling for tracer analysis is typically deemed essential for detecting tracer movement through the seepage zone. However, sampling locations may not always be accessible for all dams, especially smaller ones. Recent reports have highlighted the use of non-invasive self-potential measurements to monitor the movement of salt tracers through dam seepage zones (Bolève et al., 2011; Ikard et al., 2012). This method relies on variations in the total source current density generated by the transport of salt tracers through preferential flow paths within a dam, producing electric potential signals on the surface in response.

To conduct a more comprehensive assessment of internal erosion status, this paper introduces an experimental approach to determine the pore water velocity along the preferential flow path (local pore water velocity) based on observing the travel time of a salt tracer through self-potential anomalies on the

Authors information:
[a]Vietnam Atomic Energy Institute, Department of Nuclear Techniques, Center for Applications of Nuclear Technique in Industry, Dalat, VIETNAM. E-mail: huonghtt@canti.vn[1]; sonlv@canti.vn[2]; hieutt@canti.vn[3]; luanpt@canti.vn[4]; phungvd@canti.vn[5]; hailv@canti.vn[6]
*Corresponding Author: huonghtt@canti.vn

Received: July 30, 2022
Accepted: April 18, 2023
Published: March 31, 2024

DOI:https//doi.org/10.22452/mjs.vol43no1.2
Malaysian Journal of Science 43(1): 11-21 (Mar 2024)

ground. We investigate the suitability of self-potential anomalies in accordance with the motion of the NaCl salt tracer through a physical model experiment combined with ANSYS/CFX simulation (ANSYS Student 2021 R2). Subsequently, a salt tracer test was carried out at a leaking earthen dam in Vietnam to demonstrate the viability of the proposed approach.

2. Methodology

In the tracer experiment, tracers were injected into known locations upstream. Their occurrence at target sites downstream was monitored over time. Assuming that the adsorption effect is negligible and the tracer is instantaneously injected, the 1D analytical solution describes the tracer concentration at position *x* (m) and time *t* (s) (Evans, 1983):

$$C(x,t) = \frac{M}{A}.\frac{e^{\frac{-(x-v^{*}t)^{2}}{4.Dt}}}{\sqrt{4D\pi t}} \quad (1)$$

where *M* (kg) is the mass of the tracer, *A* is the cross-sectional area of the flow (m^2), v^* is the pore water velocity (m/s), and *D* is the dispersion coefficient (m^2/s). Considering the isotropic porous media $D = D_0/(F\phi) + \alpha v^*$, D_0 is the molecular diffusion coefficient of the tracer in solution (m^2/s), and α is the dispersivity (m).

The pore water velocity, or the mean interstitial velocity of water, is defined as the ratio between the Darcy velocity and the effective porosity. The pore water velocity can generally be determined experimentally by the following formula:

$$v^* = \frac{L}{t} \quad (2)$$

where *L* is the distance between injection and observation (m) and *t* is the time determined from the tracer breakthrough curve at the observation (s).

Previous studies have mentioned three concepts of *t* in Equation (1): t_a – the arrival time, t_p – the peak time and t_r – the mean residence time (Figure 1). The mean residence of the tracer is:

$$t_r = \frac{\int Ctdt}{\int Cdt} \quad (3)$$

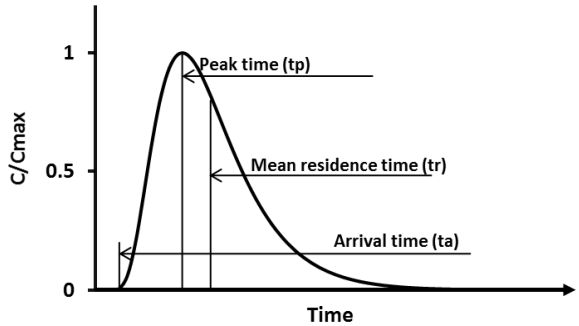

Figure 1. Examples of time characteristics of the tracer breakthrough curve: the arrival time, the peak time, and the mean residence time.

Noraee-Nejad et al. (2021) combined the consideration of the velocity determined from the arrival time (maximum velocity) and the peak time (average velocity) at piezometers to identify the primary flow direction of the preferential flow path at the Shahghasem Dam (Iran). Similarly, various t-concepts were used to assess the water volume in karst caves using the tracer method: Atkinson et al. (1973) proposed to use the peak time; Birk et al. (2004) used the arrival time; Smart (1988), Goldscheider et al. (2008) used the mean residence time; Käss (1998) concluded that when the tracer curve is severely affected by the dispersion process, using the peak time yielded better results.

When sampling locations are unavailable to observe the entire tracer curve, using a salt tracer and monitoring its movement time through the self-potential anomalies on the ground is a viable empirical approach. In this work, NaCl salt was used due to its notable advantages, such as environmental friendliness, low test cost and easy analysis. When the NaCl salt tracer moves through a porous medium, increasing the conductivity of the pore water, the source current density $\vec{j}_s$ (A.m^{-2}) generates the electric potential (Revil & Linde, 2006):

$$\vec{j}_s = \bar{Q}_v\vec{v} - \frac{K_bT}{Fe}\left(2t_{(+)} - 1\right)\nabla\sigma_f \quad (4)$$

$$\nabla.(\sigma\nabla\psi) = \nabla.\vec{j}_s \quad (5)$$

where $\vec{v}$ is the Darcy velocity (m/s); $\bar{Q}_v$ is the excess charge density (C.m^{-3}) determined from the equation $Log_{10}\bar{Q}_v = -9.2349 - 0.8219Log_{10}k$; *k* is the permeability (m^2); $K_b = 1.381\times10^{-23}$ is the Boltzmann constant (J/K); *T* is the absolute temperature (K); $F = \phi^{-m}$ is the formation factor; ϕ is the porosity; $e = 1.6022\times10^{-19}$ is the electron charge (C); $t_{(+)} = 0.38$ is the microscopic Hittorf number of the Na^+ in the pore water.; $\sigma_f = \sigma.F$ is the electrical conductivity of the pore water (S.m^{-1}); σ is the electrical conductivity of the porous

DOI:https//doi.org/10.22452/mjs.vol43no1.2
Malaysian Journal of Science 43(1): 11-21 (Mar 2024)

media (S.m^{-1}); and ψ (V) is the electric potential.

If the actual pore water velocity obtained from the tracer test is greater than the critical value, transport of soil particles within the pore structure can occur. Goltz et al. (2009) modified Wittmann's theoretical approach for the assessment of the critical velocity when taking into account adhesion and frictional forces:

$$v_{crit} = \frac{12\upsilon}{d_p\left(2.7-2.3FF\right)}\left[\sqrt{1+\left(0.21D^s\right)^3\left(2.7-2.3FF\right)\tan\varphi}-1\right] \quad (6)$$

where υ is the dynamic viscosity of water (m^2/s), FF = 0.7, d_p is the particle diameter (m), $D^s = d_p\left(\frac{\rho' g}{\upsilon^2}\right)^{1/3}$ with $\rho' = \frac{\rho_{sA}-\rho_w}{\rho_w}$, $\rho_{sA} = \rho_s + \frac{9\times10^{-8}}{d_p^{\,2}}$, ρ_s is the bulk density of soil (kg/m^3), ρ_w is the water density (kg/m^3), g is the gravitational acceleration (m/s^2), and φ is the friction angle.

3. Laboratory Experiment

The correlation between the response time of the electric potential generated by the salt migration and the travel time of water was confirmed by the salt tracer experiment on the physical model combined with numerical simulation.

Physical model

The physical model used in this study is a rectangular box with dimensions of 61.6 cm x 30 cm x 30.8 cm, constructed from 0.8 cm-thick sheet glass. The model was divided into three compartments by two 1 cm thick mica sheets with holes drilled 1 cm in diameter and a distance of 2 cm between holes. Two 10 cm long compartments at the ends act as upstream and downstream reservoirs, while the 38 cm long compartment in the middle is packed with glass beads. Fabric mesh with a mesh diameter of 100 µm was attached to the two shields to prevent glass beads from spilling into the other two compartments. The total height of the glass bead column is 20 cm. The porosity of the middle compartment is 37%. The flow through the porous media is controlled by the water levels of the upstream and downstream. Upstream water was supplied by a water tank located 3 m above the ground and a tube with a diameter of 1 cm. The supplying flow rate was regulated with a valve. The downstream water level was adjusted by changing the outlet height of the 1 cm diameter overflow discharge tube. The experiment used tap water as the fluid with an average conductivity of 2.4x10^{-3} S·m^{-1}. We used laboratory glass beads with a diameter of about 450-500 µm. By measuring the outlet flow rate according to the difference in water level, the permeability was determined to be 1.95x10^{-10} m^2. The experimental system and the sketch of the physical model are shown in Figures 2a and 2b.

The laboratory Cu/$CuSO_4$ electrodes, in combination with a Fluke 87V voltmeter (USA), were used to record the electric potential during the transport of the NaCl tracer. The in-house electrodes operate with a natural drift of 0.02 mV/min (22°C). The dependence of the potential drift on ambient temperature was ignored because the temperature fluctuation in the experiment is insignificant (within 0.1°C). A total of three electrode arrays (four electrodes each array) were inserted into the middle compartment (depth 8.5 cm from the top), and the reference electrode was placed upstream at (x; y) = (0 cm; 14.5 cm). The position of the electrodes is considered in the Cartesian coordinate system with the x-axis parallel to the flow direction and the y-axis perpendicular to it. The electrode arrays have coordinates y = (6.5 cm; 14.5 cm; 22 cm), with the positions of the measuring electrodes along the x-axis being (6.5 cm; 14.5 cm; 23 cm; 31.5 cm), as shown in Figure 2c.

DOI:https//doi.org/10.22452/mjs.vol43no1.2
Malaysian Journal of Science 43(1): 11-21 (Mar 2024)

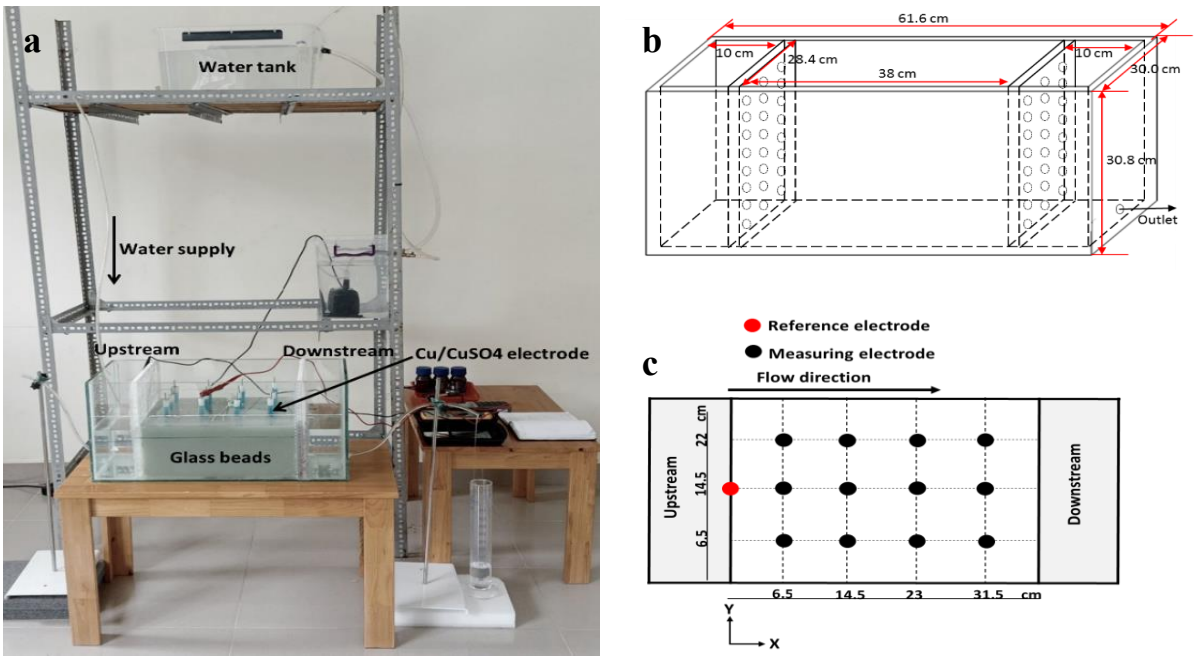

Figure 2. The experimental system: (a) Photo of experimental system; (b) Sketch of physical model; (c) Illustration of electrode position (top view).

Experimental Procedure

The upstream level was maintained at 20 cm, and the tracer experiment was carried out with a flow rate of 0.81 L/min, corresponding to a 17 cm downstream level. The pore water velocity, calculated from the ratio between the Darcy velocity and the effective porosity, was 3.85 cm/min.

After setting the downstream and upstream levels, the experimental system was stabilized for several hours. Before the injection of the tracer, the potential difference between the 12 measuring electrodes and the reference electrode was recorded. This included the signal generated by the steady flow in the model and the difference in internal potential between the electrodes. Simultaneously, the initial conductivity of the water was measured to establish a background value. A total of 120 mL of the salt tracer solution, containing 4.42 g of NaCl, was injected into the upstream reservoir, which had a water volume of 5.68 L. The potential difference between the reference and measuring electrodes was recorded over time using a Fluke 87V voltmeter (USA). The measuring time for the 12 electrodes was 20 seconds, with a measurement frequency of 1 minute. The NaCl concentration over time at the downstream drainage was measured using a conductivity meter, specifically a Hanna HI98197 device (Romania). The linear relationship between the concentration of Cl^- (C, in mg/L) and the conductivity of water (EC, in µS/cm) is represented by the equation C = 0.25EC – 4.49, with an R^2 value of 0.998. The initial electric potential before tracer injection and the natural drift potential were subtracted from the measurement data. The temperature during the experiment remained stable within a range of 21.9°C to 22.1°C.

ANSYS/CFX Simulation

A multi-component numerical model was developed to analyze the concentration distribution of the tracer and correlate it with the variations in the experimental electric potential. This model simulates the movement of the NaCl tracer within the physical model over time and was constructed using the ANSYS/CFX software, specifically the ANSYS Student 2021 R2 version. In this multi-component model, the fluid, comprising multiple components, is treated as an ideal mixture. This means that the fluid's velocity, pressure, and temperature are computed by solving the continuity equation and the Navier-Stokes equations. For this experiment, the fluid system includes two main components: water and a solution of the NaCl tracer. The advection-dispersion equation is solved following the determination of the fluid's velocity field. This process enables the determination of the tracer's movement through the medium, allowing for a detailed examination of its distribution over time.

DOI:https//doi.org/10.22452/mjs.vol43no1.2
Malaysian Journal of Science 43(1): 11-21 (Mar 2024)

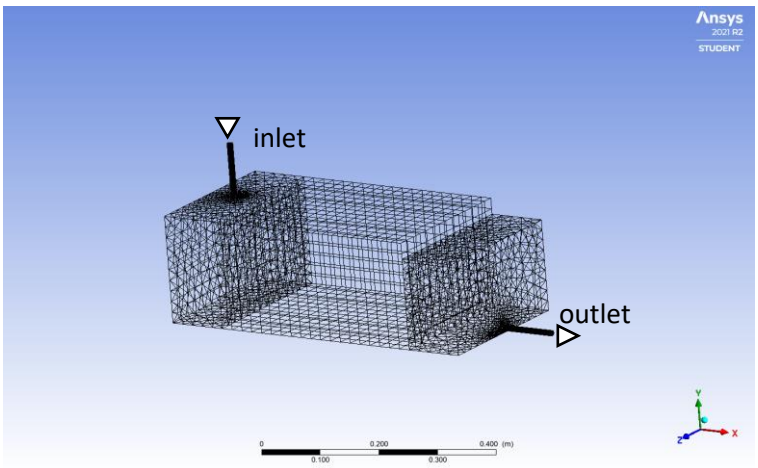

Figure 3. The structured mesh of the model (courtesy of ANSYS, Inc.)

The numerical simulation involved a substantial computational mesh comprising 58,926 elements and 15,934 nodes, as depicted in Figure 3. The simulation process was divided into two main steps to ensure accuracy and comprehensiveness. Initially, the model was brought to a steady state by achieving convergence in the velocity field. This phase was capped at a maximum of 600 iterations, with convergence being determined by meeting the Residual RMS criterion of $1x10^{-4}$. At both the inlet and outlet, velocity boundary conditions were implemented based on experimental data, with the velocity vector directed normally to the boundary surfaces. Furthermore, an open boundary condition was applied at the top of the porous region, designed to permit air to traverse the boundary surface perpendicularly, thus simulating a realistic environmental interaction.

Following the establishment of a steady state, the simulation transitioned to a transient phase to model the injection of the NaCl solution. This phase used the outcome of the steady-state simulation as its input file. Initially, the NaCl solution concentration was set to zero throughout the domain. During the tracer injection period ($0 \leq t \leq t_0$, where t_0 represents the injection stop time), the mass fraction of the tracer in the fluid at the inlet was maintained at 1, with a time step size (Δt) of 0.2 seconds. For times $t > t_0$, the tracer concentration was set to zero, and the time step size was adjusted to 1 second to simulate the cessation of tracer injection, aligning with the experimental procedure.

The maximum number of iterations per time step during the transient simulation was limited to 10, adhering to the same convergence criteria established for the steady-state model. The turbulence effects within the fluid flow were modeled using the k-Epsilon turbulence model, with a default turbulence intensity of 5% at both the inlet and outlet, ensuring a realistic simulation of fluid dynamics within the system.

4. Field-Scale Experiment

The study dam was built in 1997 in the Dong Nai river basin, situated approximately 200 km northeast of Ho Chi Minh City. It is a homogeneous earth-fill dam with a height of 36 m and a crest length of 215 m. The physical characteristics of the soil embankment are shown in Table 1.

Table 1. The physical characteristics of the soil embankment.

Density (kg/m^3)	Particle diameter (m)	Friction angle (degrees)	Hydraulic conductivity (m/s)
1870	$5.0x10^{-6}$	20.0	$2.0x10^{-8}$

According to the company's report, a wet area downstream of the dam becomes evident when the reservoir water level surpasses 604 meters. This area, measuring approximately 7 meters by 3 meters, is located at 595 meters, as illustrated in Figure 4a. In December 2021, in collaboration with the dam supervisor, a ditch was constructed to collect seepage water. This water was then directed into a measurement hole with dimensions of 40 cm by 40 cm by 15 cm to assess the leak's flow rate. The findings indicated that the leakage flow rate was 0.5 liters per minute when the reservoir's water level reached 605 meters.

To ascertain the direction and local pore water velocity of preferential flow paths through the dam, a salt tracer test was conducted. On December 18, 2021, nylon bags filled with NaCl tracer crystals were placed into the reservoir. These bags, positioned 78 meters symmetrically from the leak site (as depicted in Figure 4b), were perforated, allowing the salt crystals to dissolve gradually into the reservoir water. Each bag,

DOI:https//doi.org/10.22452/mjs.vol43no1.2
Malaysian Journal of Science 43(1): 11-21 (Mar 2024)

containing 5 kg of NaCl, was submerged at a depth of 1 meter and spaced 3 meters apart. At the time of the tracer injection, the reservoir water level was recorded at 604.6 meters. Over approximately three hours post-injection, the electrical conductivity and chloride ion (Cl^-) concentration were measured at various distances from the injection point. The leakage site offered the sole opportunity for downstream sampling. Water samples were collected until February 3, 2022, for analysis of conductivity and Cl^- concentration at the Laboratory (VILAS-609) of the Center for the Application of Nuclear Techniques in Industry. To prevent air contact, 300 mL water samples were sealed in plastic bottles. The Cl^- concentration was determined using test method TCVN 6494-1:2011, with a minimum detection limit of 0.01 mg/L. A Hanna HI98197 instrument (Romania) with a resolution of 0.1 µS/cm was used to measure the electrical conductivity of the samples. Prior to the tracer injection, the Cl^- concentration in the reservoir water was 3.80 mg/L and in the leak water was 2.77 mg/L, correlating to conductivities of 66.5 µS/cm and 28.5 µS/cm, respectively.

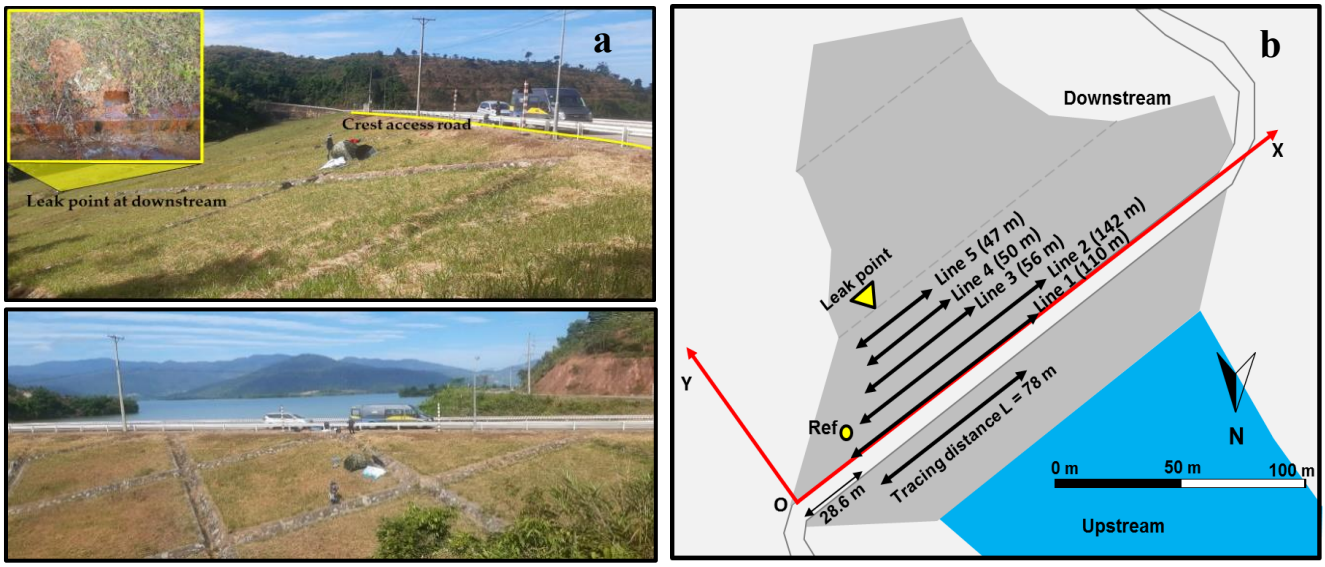

Figure 4. (a) The study dam site; (b) The tracing distance, measuring lines for electric potential (Line 1-5), and reference electrode (Ref) position.

A comprehensive electric potential measurement campaign was conducted at the dam site involving five measuring lines (Line 1-5) before and after the injection of a salt tracer. The initial measurements took place on December 17, 2021, with subsequent sessions on January 5, January 18, and January 26, 2022. These measuring lines were laid out parallel to the toe of the dam downstream, spaced 10 meters apart from each other. To enhance efficiency and reduce the survey time, the length of the measuring lines was decreased moving downstream.

Measurements were carried out using a pair of non-polarized $Cu/CuSO_4$ electrodes, which were connected to a measuring device capable of handling a maximum impedance of 20 MΩ and equipped with a 500 m cable, specifically the ARES II measurement system by GF Instruments. The reference electrode was stationed at the left abutment of the dam (as shown in Figure 4b), while the other electrode was moved to each measurement point along the measuring lines. The average spacing between measurement points was 8 meters, though adjustments were made based on the ground conditions encountered at each site. At every measurement location, a small hole approximately 10 cm deep was dug to ensure contact with moist soil, facilitating accurate measurements.

Given the $Cu/CuSO_4$ electrodes' sensitivity to temperature fluctuations, protective measures were taken to shield the electrodes from direct sunlight during measurements, including a mandatory pre-measurement waiting period of 5 minutes at each point to ensure temperature stabilization. At each measurement point, five readings were taken, with the average relative error recorded at 1.7%. Additionally, the drift potential of the electrodes was assessed at the beginning and end of each measuring line while they were immersed in a bath of saturated $CuSO_4$ solution, registering a potential value around 1 mV.

Consistent with findings from previous research, such as that by Revil et al. (2003), corrections for telluric currents were deemed unnecessary for this study due to the short temporal span and limited geographical scale (below 1 km) of the measurements. Consequently, the collected raw electric potential data were adjusted for the drift potential across each measuring line, ensuring the accuracy of the data analysis.

DOI:https//doi.org/10.22452/mjs.vol43no1.2
Malaysian Journal of Science 43(1): 11-21 (Mar 2024)

5. Results and Discussion

Laboratory Experiment Results

Figure 5a illustrates a comparative analysis between the tracer response curves at the outlet, as obtained from both ANSYS/CFX simulations and experimental observations. The numerical model's accuracy was validated through a root-mean-square error (RMSE) of $1x10^{-4}$ between the simulation outputs and the experimental data. Figure 5b presents a comparison of the experimental electric potential signals recorded at distances of x = 6.5 cm, 14.5 cm, 23 cm, and 31.5 cm with the tracer curves derived from simulation results.

The temporal distribution of electric potential at these measuring positions mirrors the findings of Maineult and Bernabé (2005), showcasing a notable pattern. Immediately following tracer injection, there's a rapid decline in the electric potential to negative values, followed by a swift transition through zero, eventually stabilizing over time. This abrupt shift in electric potential corresponds closely with the arrival times of the water at each measuring point, demonstrating the direct influence of water movement on electric potential signals.

The observed travel times for the water to reach the respective measuring positions were 1.7, 3.8, 6, and 8.2 minutes, correlating to positions x = 6.5 cm, 14.5 cm, 23 cm, and 31.5 cm, respectively. These times align with a calculated pore water velocity (v*) of 3.85 cm/min. Such detailed comparison not only confirms the predictive accuracy of the numerical model but also provides valuable insights into the dynamics of tracer movement and its interaction with the electric potential field within the experimental setup.

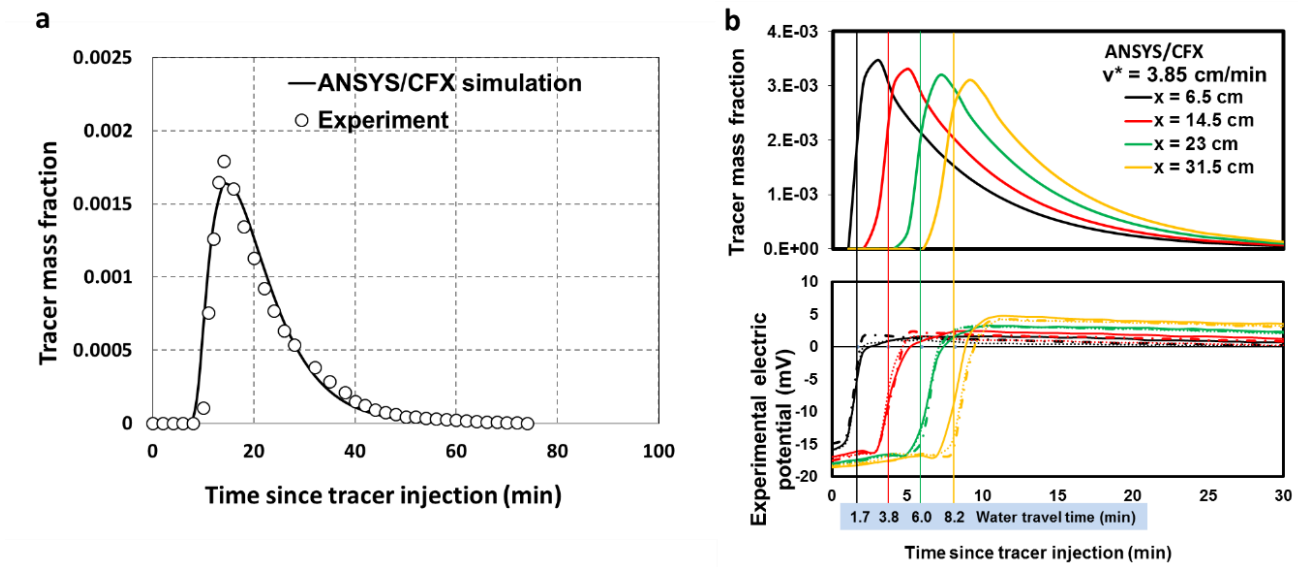

Figure 5. (a) The tracer response curve at the outlet obtained from ANSYS/CFX simulation and experiment; (b) The electric potential signal at measuring positions of *x* = 6.5 cm, 14.5 cm, 23 cm, 31.5 cm. The corresponding tracer curves were determined from the simulation.

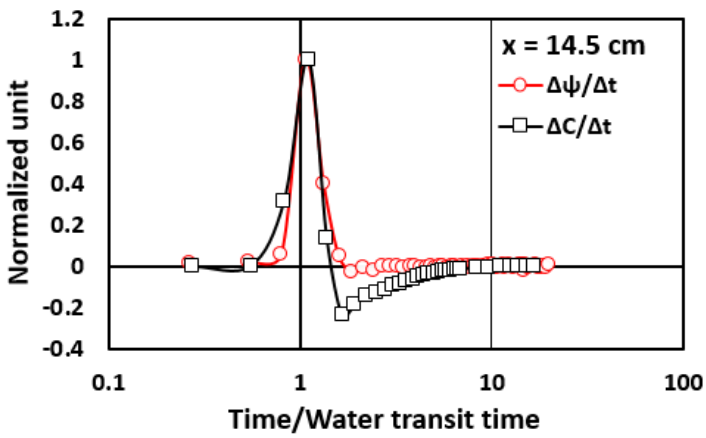

Figure 6. The maximum potential variation $(\Delta\Psi/\Delta t)_{max}$ and the change in tracer curve $(\Delta C/\Delta t)_{max}$ coincide in time and are close to the water transit time.

DOI:https//doi.org/10.22452/mjs.vol43no1.2
Malaysian Journal of Science 43(1): 11-21 (Mar 2024)

Due to the tracer dispersion effect by dilution at the input boundary, the travel time of water is earlier than the time to reach the maximum tracer concentration (Figure 5b). Experimental and simulation results demonstrate that the change in tracer curve $(\Delta C/\Delta t)_{max}$ agrees with the maximum potential variation $(\Delta \Psi/\Delta t)_{max}$ and is close to the water transit time, as illustrated in Figure 6.

Figure 7 shows the position of the tracer plume derived from ANSYS/CFX (ANSYS Student 2021 R2) (the plane z = 10 cm) relative to the location of the experimental electric potential anomalies at 4, 6, and 8 min. The electric potential signal anomalies were considered by analyzing the signal variation ($\Delta \Psi/\Delta t$, in mV/min). The results demonstrate that the location of the electric potential anomaly is relatively consistent with the position of the tracer plume. The centroid positions of the tracer plume are x = 11 cm, 19 cm, and 27 cm at 4, 6, and 8 min, respectively. The mean deviation of the peak potential anomaly location and the center of the tracer plume is 4 cm (about 10.5% of the total travel distance). The occurrence time of the signal anomaly at a location is close to the actual water travel time. Calculation results of pore water velocity were based on two approaches: (1) the location of the tracer plume determined from ANSYS/CFX, and (2) the location of the potential signal anomaly (Table 2). The calculated velocities show an error of about 10% if the water moving distance was measured from the center of the tracer plume, and an error of 6% if the water moving distance was measured from the position of the maximum potential anomaly.

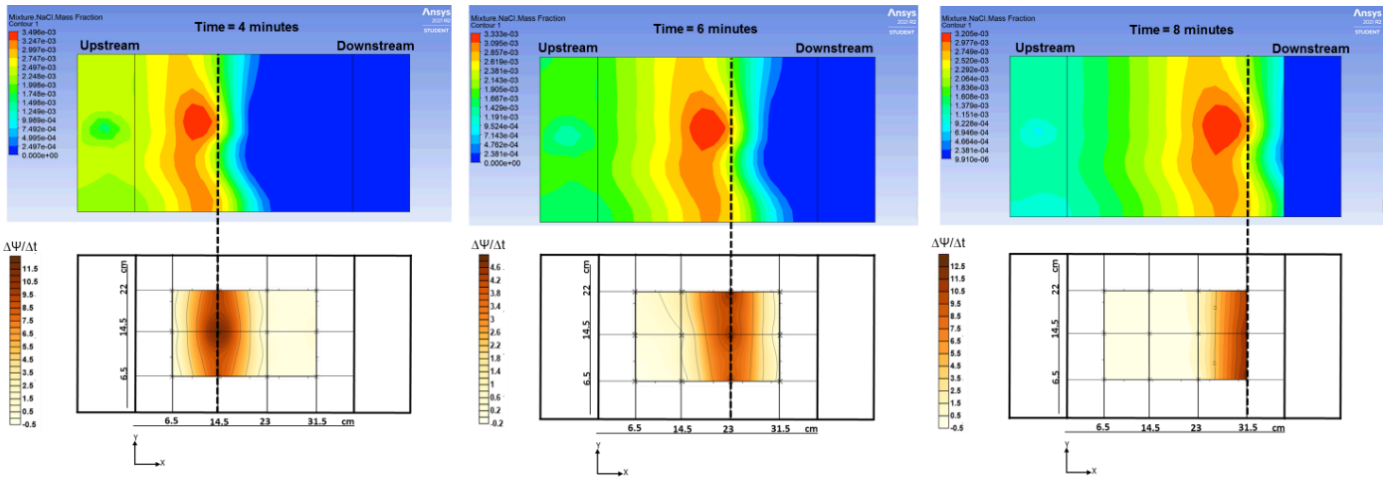

Figure 7. Positions of the tracer plume obtained from ANSYS/CFX (the plane z = 10 cm) compared to the self-potential anomalies. It is shown that tracer plumes are consistent with self-potential signal anomalies (courtesy of ANSYS, Inc.).

Table 2. Calculation results of pore water velocity of the model.

Observation time	4 min	6 min	8 min
Tracer travel distance			
Centroid position of the tracer plume	11 cm	19 cm	27 cm
Position of the maximum electric potential anomaly	14.5 cm	23 cm	31.5 cm
Pore water velocity			
Centroid position of the tracer plume	2.75 cm/min	3.17 cm/min	3.38 cm/min
Position of the maximum electric potential anomaly	3.63 cm/min	3.83 cm/min	3.93 cm/min

Field-Scale Experiment Results

The introduction of the NaCl tracer into the reservoir water at an elevation of 604.5 m allowed for precise monitoring and analysis of its dispersion and eventual seepage through the dam. The measurement of electrical conductivity and Cl^- concentration in the reservoir water at intervals of 0.8 hours, 1.8, 2.8, and 3.3 hours post-injection, as illustrated in Figure 8a, aimed to identify the seepage leakage inlet of the dam. The inlet is hypothesized to be the location where the concentration of the tracer peaks after a period of diffusion, indicating the most significant point of seepage.

The results from these measurements revealed that the peak conductivity and Cl^- concentration were observed approximately 42 meters from the point of tracer injection. This peak indicates the likely inlet of seepage through the dam, where the tracer concentration was highest. Following 3.3 hours after injection, the conductivity in the reservoir water approached the background levels again, suggesting the dispersion of the tracer away from the peak concentration point over time.

Figure 8b details the analysis of electrical conductivity and Cl^- concentration at the leak point itself, revealing the tracer's

DOI:https//doi.org/10.22452/mjs.vol43no1.2
Malaysian Journal of Science 43(1): 11-21 (Mar 2024)

response curve in the form of a single peak. Remarkably, the peak occurred 40 days after the tracer was introduced, with the highest recorded conductivity value at 118.70 µS/cm, which corresponds to a Cl^- concentration of 28.06 mg/L. This significant delay in reaching the peak concentration at the leak point underscores the slow movement of water through the dam's structure, providing critical insights into the dynamics of seepage and the efficacy of tracer tests in identifying and analyzing potential leakage paths within dam infrastructures.

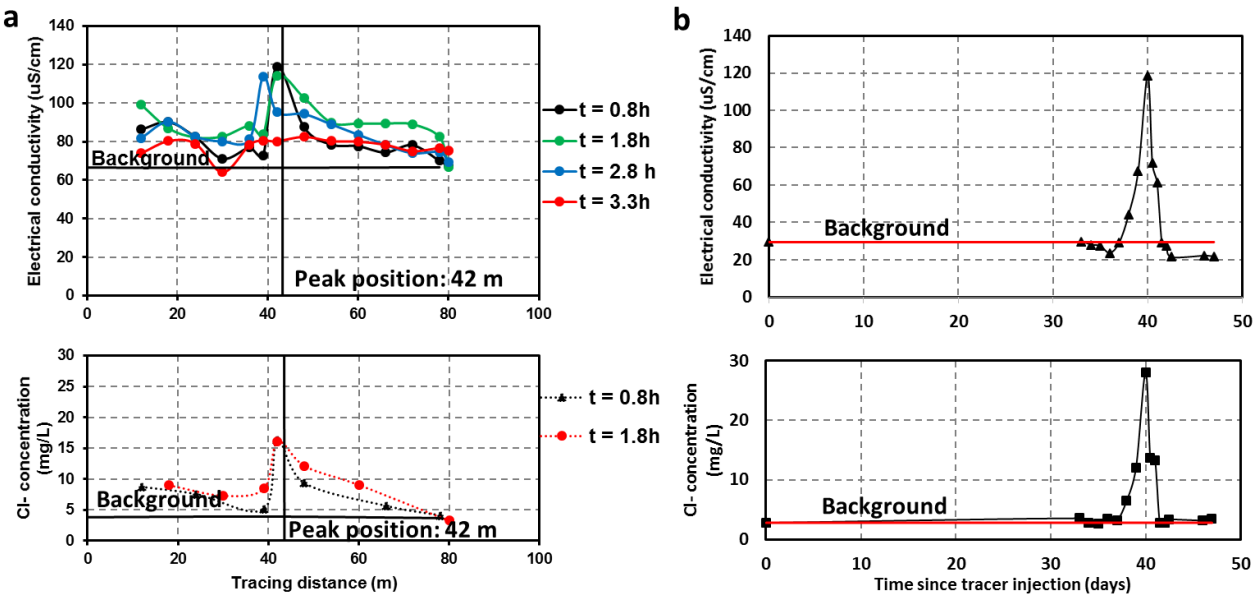

Figure 8. Results of salt tracer test at the study dam: (a) Measurement results of electrical conductivity and Cl^- concentration in reservoir water at 0.8, 1.8, 2.8, and 3.3 hrs after injection; (b) Electrical conductivity and Cl^- concentration in water at the leak point over time.

The potential anomaly is indicated by the signal variation ($\Delta\Psi/\Delta t$) quantity. By comparing the potential signal variation before and after under the same field-scale conditions, the distinctive region associated with the presence of salt ions can be easily identified. Figure 9 presents the results of electric potential anomalies at the dam after 18, 30, and 40 days since the injection. The location of the anomaly that indicates the direction of the tracer movement from upstream to the leak point has a horizontal V-shape. The travel time of the salt tracer from upstream (position 1) to Line 2 (position 2) is 18 days, from Line 2 (position 2) to Line 5 (position 3) is 12 days, and from Line 5 (position 3) to the leak point is ten days. Based on the distance of movement, the local pore water velocity is presented in Table 3.

The local pore water velocity ranges from 1.2×10^{-5} m/s to 7.0×10^{-5} m/s. The calculation results demonstrate that the velocity in the 2 - 3 position range is the greatest. Taking into account the tortuosity of the porous medium, the actual velocity of the water is proportional to the actual distance travelled $L_a = L\tau$, where τ is the tortuosity. The actual velocity results are presented in Table 2 with τ = 1.4 (Freeze & Cherry, 1979). The critical velocity, which causes internal erosion, was estimated using Equation (6) with the physical characteristics of the soil embankment (Table 1) as 2.5×10^{-5} m/s (υ = $0{,}8927\times10^{-6}$ m²/s at 25°C and ρ_w = 997 kg/m³ at 25°C). It can be seen that the pore water velocity in the 2 - 3 position range is approximately four times greater than the critical value.

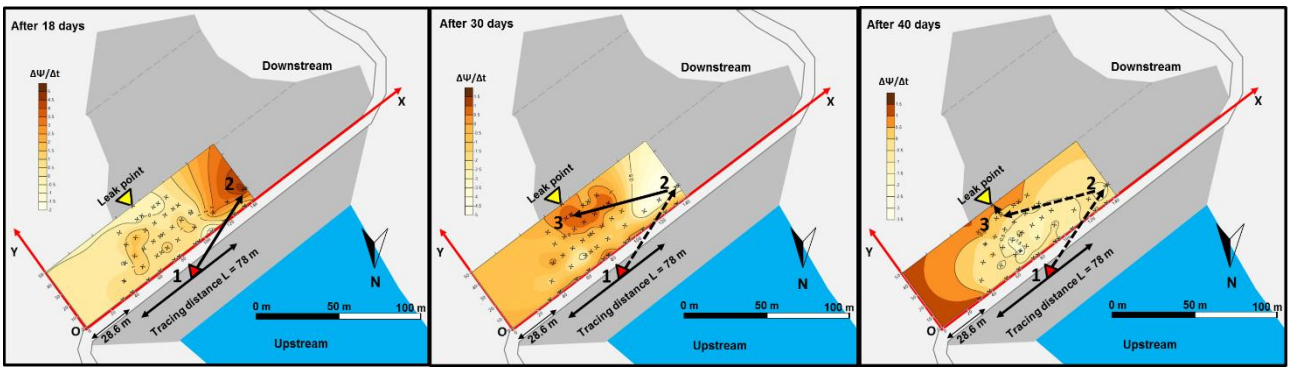

Figure 9. Location of electric potential anomalies at the study dam after injection: 18, 30, and 40 days. Position 1 is conventionally the leakage inlet, determined at the point where the conductivity/Cl^- concentration peaks after injection.

DOI:https//doi.org/10.22452/mjs.vol43no1.2
Malaysian Journal of Science 43(1): 11-21 (Mar 2024)

Table 3. Local pore water velocity along the preferential flow of the study dam.

Position	Travel distance (m)	Travel time (days)	Local pore water velocity (m/s)	Actual pore water velocity (m/s)
1-2	77.8	18	$5.0x10^{-5}$	$7.0x10^{-5}$
2-3	73.0	12	$7.0x10^{-5}$	$9.9x10^{-5}$
3-Leak point	10.4	10	$1.2x10^{-5}$	$1.7x10^{-5}$

6. Conclusion

This study introduced a novel approach to evaluating the local pore water velocity of preferential flow paths through porous media by monitoring the movement of a NaCl salt tracer and observing the associated electric potential anomalies on the ground. Experiments conducted on a physical model demonstrated a close correlation between the timing of signal variations and the movement of water to the measuring positions. Additionally, the distribution of the salt tracer plume, as determined from ANSYS/CFX simulations, aligned well with the observed positions of electric potential anomalies over time. The pore water velocity, inferred from the location exhibiting the maximum electric potential anomaly, showed consistency with the experimental values, boasting an error margin of less than 6%.

A field-scale salt tracer experiment conducted at a leaking earth dam in Vietnam further underscored the practicality of this method. The tracer response curve obtained from the leak site revealed that the seepage water's transport time was approximately 40 days. Following tracer injection, the electric potential anomalies provided insight into the preferential flow path from upstream to the leak point and enabled the estimation of local pore water velocities.

This methodological approach presents a significant advancement in assessing internal erosion caused by seepage within earthen dams, utilizing the criterion of pore water velocity. It offers substantial benefits over traditional methods, notably in terms of cost-effectiveness and the ability to overcome challenges associated with sample collection for tracer analysis at the field site. This technique not only aids in the precise identification of seepage paths and velocities but also enhances the capability to effectively manage and mitigate risks associated with dam integrity and safety.

7. Acknowledgement

This work was supported by the Vietnam Ministry of Science and Technology. The authors also show gratitude to ANSYS Inc. for introducing the free version for academic purposes.

6. References

Atkinson, T.C., Smith, D.I., Lavis, J.J., and Whitaker, R.J. (1973). Experiments in tracing underground waters in limestones. Journal of Hydrology, 19, 323–349.

Battaglia, D., Birindelli, F., Rinaldi, M., Vettraino, E., Bezzi, A. (2016). Fluorescent tracer tests for detection of dam leakages: The case of the Bumbuna dam - Sierra Leone. Engineering Geology, 205, 30–39.

Bedmar, A.P, Araguas, L. (2002), Detection and Prevention of Leaks from Dams. A.A. Balkema Publishers.

Bigman, D.P, Day, D.J. (2022). Ground penetrating radar inspection of a large concrete spillway: A case-study using SFCW GPR at a hydroelectric dam. Case Studies in Construction Materials, 16, e00975.

Birk, S., Liedl, R., and Sauter, M. (2004). Identification of localized recharge and conduit flow by combined analysis of hydraulic and physio-chemical spring responses (Urenbrunnen, SW Germany). Journal of Hydrology, 286, 179-193.

Bolève, A., Janod, F., et al. (2011). Localization and quantification of leakages in dams using time-lapse self-potential measurements associated with salt tracer injection. Journal of Hydrology, 403, 242–252.

Evans, G. V. (1983). Tracer Techniques in Hydrology. Int. J. Appl. Radiat. Lsot, 34(I), 451-475.

Foster, M., Fell, R., & Spannagle, M. (2000). The statistics of embankment dam failures and accidents. Canadian Geotechnical Journal, 37(5), 1000-1024.

Freeze, R. A, Cherry, J. A. (1979). Groundwater. Prentice-Hall, Englewood Clifs.

Goldscheider, N., Meiman, J., Pronk, M., & Smart, C. (2008). Tracer tests in karst hydrogeology and speleology. International Journal of Speleology, 37(1), 27-40.

Goltz, M., Etzer, T., Aufleger, M., & Muckenthaler, P. (2009, 12-23 October). Assessing the critical seepage velocity causing transport of fine particles in embankment dams and their foundation, Long term behaviour of dams proceeding of the 2nd international conference, Graz, Austria, (pp.479-484).

Hickey, C.J., Ekimov, A., Hanson, G., & Sabatier, J., (2010). Time-Lapse Seismic Measurements on a Small Earthen Embankment During an Internal Erosion Experiment. In SAGEEP 2009 Proceedings. Keystone, Colorado.

DOI:https//doi.org/10.22452/mjs.vol43no1.2
Malaysian Journal of Science 43(1): 11-21 (Mar 2024)

Hui, L., Haitao, M. (2011). Application of Ground Penetrating Radar in Dam Body Detection. Procedia Engineering, 26, 1820 – 1826.

Ikard, S. J., Revil, A., et al. (2012). Saline pulse test monitoring with the self-potential method to nonintrusively determine the velocity of the pore water in leaking areas of earth dams and embankments. Water Resource Research, 48(W04201).

Käss, W. (1998). Tracing Technique in Geohydrology. Rotterdam, Balkema, 581.

Kukemilks, K., Wagner, J.-F. (2021). Detection of Preferential Water Flow by Electrical Resistivity Tomography and Self-Potential Method. Appl. Sci, 11, 4224.

Maineult, A., Bernabé, Y. (2005). Detection of advected concentration and pH fronts from self-potential measurements. Journal of Geophysical Research, 110(B11205).

Noraee-Nejad, S., Sedghi-Asl, M., Parvizi, M., Shokrollahi, A. (2021). Salt tracer experiment through an embankment dam. Iranian Journal of Science and Technology, Transactions of Civil Engineering.

Qiu, H., Hu, R., Huang, Y., Gwenzi, W. (2022). Detection and Quantification of Dam Leakages Based on Tracer Tests: A Field Case Study. Water, 14, 1448.

Revil, A., Linde, N. (2006). Chemico-electromechanical coupling in microporous media. Journal of Colloid and Interface Science, 302, 682–694.

Revil, A., Naudet, V., Nouzaret, J., & Pessel, M. (2003). Principles of electrography applied to self-potential electrokineticsources and hydrogeological applications. Water resources research, 39(5), 1114.

Smart, C.C. (1988). Quantitative tracing of the Maligne karst system, Alberta, Canada. Journal of Hydrology, 98, 185–204.

Zhang, L., Peng, M., Chang, D., & Xu, Y. (2016). Dam Failure mechanisms and risk assessment. John Wiley & Sons Singapore Pte. Ltd.

Zumr, D., David, V., Jeřábek, J., Noreika, N & Krása, J. (2020). Monitoring of the soil moisture regime of an earth-filled dam by means of electrical resistance tomography, close range photogrammetry, and thermal imaging. Environ Earth Sci, 79, 299.

DOI:https//doi.org/10.22452/mjs.vol43no1.2
Malaysian Journal of Science 43(1): 11-21 (Mar 2024)